Draft version August 1, 2017
Typeset using LaTeX **twocolumn** style in AASTeX61

LET THERE BE LIGHT: EARLY OBSERVATIONS OF THE NORMAL TYPE IA SUPERNOVA iPTF 16abc SHOW NO EVIDENCE FOR A DARK PERIOD

The Alphabet Friends[1]

[1] *the intermediate Palomar Transient Factory*

(Received August 1, 2017; Revised; Accepted)

Submitted to ApJ

ABSTRACT

Early observations of Type Ia supernovae (SNe) provide a unique probe of their progenitor systems and explosion physics. Here, we report the intermediate Palomar Transient Factory (iPTF) discovery of an extraordinarily young SN Ia, iPTF 16abc. The initial detection was made only $0.18\pm^{0.07}_{0.15}$ d after SN first light. In the $\sim$24 hr after discovery, iPTF 16abc rose by $\sim$2 mag, following a near-linear rise in flux for $\sim$4 d. Assuming the photospheric velocity follows a $t^{-0.22}$ power law, the time of explosion for iPTF 16abc is approximately equal to the time of first light. Strong C II absorption is detected in the early spectra of iPTF 16abc, before disappearing after $\sim$7 d. Unlike SN 2011fe, the $(B-V)_0$ colors of iPTF 16abc are blue and nearly constant in the days after explosion. We show that the fast, near-linear rise in flux for iPTF 16abc cannot be explained by either SN shock breakout and the associated, subsequent cooling or the collision of the SN ejecta with a stellar companion. Instead, we argue that the early characteristics of iPTF 16abc, including: (i) the rapid, near-linear rise, (ii) the non-evolving blue colors, and (iii) the strong lines from ionized carbon in the earliest spectra, are the result of either vigorous mixing of radioactive ^{56}Ni in the SN ejecta, or the interaction of the ejecta with diffuse material, or a combination of the two. In the next few years, dozens of very young *normal* SNe Ia will be discovered, and observations similar to those presented here will constrain the white dwarf explosion mechanism.

Keywords: methods: observational — supernovae: individual (iPTF 16abc)

Corresponding author: A. A. Miller
amiller@northestern.edu

1. INTRODUCTION

Although Type Ia supernovae (SNe Ia) have been extensively used as standardizable candles, their progenitor systems and explosion physics are still debated (see a recent review by Maoz et al. 2014). Extremely detailed observations in the hours to days after explosion are one of the most promising avenues to further constrain this problem.

While the shock breakout of a SN Ia occurs on a subsecond timescale, the subsequent quasi-adiabatic expansion and cooling of the unbound ejecta produces thermal emission that can be used to infer the radius of the exploding star (Piro et al. 2010; Rabinak & Waxman 2011). Comparing models of this cooling emission to the earliest-phase data of SN 2011fe, Bloom et al. (2012) concluded that the explosion came from a star with $R_* \lesssim 0.02 R_\odot$, where $R_\odot$ is the solar radius. Combining the radius constraint with the measured ejecta mass Bloom et al. derive the mean density of the progenitor star, confirming that at least some type Ia SNe come from compact and degenerate stars.

Early phase observations of SNe Ia from a white dwarf (WD)+non-degenerate binary may detect excess emission, relative to most type Ia SNe, due to the collision of the SN ejecta with the non-degenerate companion (Whelan & Iben 1973; Kasen 2010). This excess emission was first detected in iPTF 14atg (Cao et al. 2015), a low-velocity SN Ia with a significant and declining ultraviolet (UV) pulse detected within a few days of the SN explosion. This UV pulse is best interpreted as a SN ejecta-companion collision. While such emission requires a favorable geometric alignment and is only expected in $\lesssim 10\%$ of SNe Ia (Kasen 2010), many studies have searched for signatures of an ejecta-companion interaction, typically resulting in non-detections (e.g., Hayden et al. 2010a; Bianco et al. 2011; Foley et al. 2012; Bloom et al. 2012; Olling et al. 2015; Zheng et al. 2013; Goobar et al. 2015; Shappee et al. 2016b; Im et al. 2015). Possible exceptions include SN 2012cg, which exhibited excess blue emission in its early-phase light curve (Marion et al. 2016; though see Shappee et al. 2016a for an interpretation that does not invoke ejecta-companion interaction), and SN 2017cbv, which shows a clearly resolved "bump" in the early UBg light curves (Hosseinzadeh et al. 2017).

Interaction is not limited to systems with a non-degenerate companion, however, as WDs enshoruded in diffuse material following a binary merger or expanded due to a pre-explosion pulsation can give rise to ejecta-interaction signatures (see e.g., Dessart et al. 2014). Models of this scenario naturally produce C II absorption that is comparable in strength to Si II in the days after explosion (Dessart et al. 2014), as was observed in SN 2013dy (Zheng et al. 2013) and SN 2017cbv (Hosseinzadeh et al. 2017).

The vast majority of SNe Ia are observed to be powered purely by the radioactive decay of ^{56}Ni. While the detection of SN shock cooling or ejecta interaction is rare, the level of ^{56}Ni mixing in the SN ejecta can fundamentally alter the appearance of the SN shortly after explosion. SNe Ia experience a dark period after the SN shock breakout but before radioactive energy diffuses into the photosphere (Piro & Nakar 2014). The duration of this dark period is set by how the newly synthesized ^{56}Ni is mixed and deposited into different layers of the ejecta. In the case of strong mixing, the dark period is short, or non-existent, as photons from ^{56}Ni decay can reach the photosphere rapidly. This also leads to blue optical colors and a rapid initial rise in the observed light curve. If the mixing is weak and the ^{56}Ni is confined to the innermost layers of the ejecta, the dark period can last for several days as the radioactive energy diffuses to the photosphere. The early evolution of such SNe results in redder colors and a more moderate rise in luminosity (Piro & Morozova 2016). Thus, the early light curves of even non-exotic type Ia SNe convey information about their progenitor systems by constraining the distribution of synthesized ^{56}Ni, which in turn constrains the explosion mechanism.

In this paper, we report observations of an extraordinarily young SN Ia, iPTF 16abc, which was discovered by the intermediate Palomar Transient Factory (iPTF) on 2016 April 3.36[1] at R.A. = $13^h34^m45.49^s$, Dec. = $+13^d51^m14.3^s$ (J2000) with a $g_{\rm PTF}$-band magnitude of 21.31 ± 0.27 (Miller et al. 2016). The transient is spatially coincident with a tidal tail of the galaxy NGC 5221, which lies at a distance of $\sim$100 Mpc. iPTF 16abc is not detected to a limit of $g = 22.1$ mag on April 2.42, less than 1 d prior to discovery, and rose by $\sim$2 mag in the 24 hr following its initial detection. Our spectroscopic follow-up campaign classified iPTF 16abc as a normal SN Ia (Cenko et al. 2016). Our observations and analysis show that the early evolution of iPTF 16abc exhibited several distinct properties relative to SN 2011fe. We interpret those differences as arising from either strong ^{56}Ni mixing or ejecta interaction with diffuse material, or a combination of the two.

2. OBSERVATIONS

During the spring of 2016, the iPTF survey observed the field of iPTF 16abc every night in either the $g_{\rm PTF}$- or

[1] All times in this paper are in UTC.

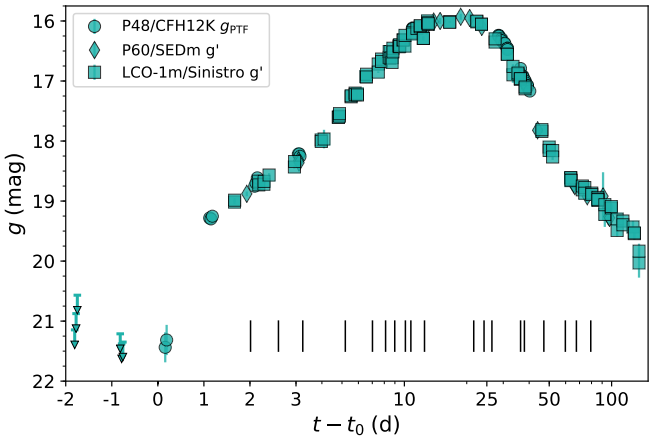

Figure 1. The g-band light curve of iPTF 16abc. Observations from different telescopes are shown with different symbols. Time is measured in rest-frame d relative to the time of first light, t_0 (see §4.1). Note that the horizontal axis is shown with a linear scale for -2 d $\leq t - t_0 \leq 3$ d and a log scale for $t - t_0 > 3$ d. The black ticks near the bottom of the panel show epochs of spectroscopic observations.

$R_{\rm PTF}$-band.[2] Survey observations were conducted with the CFH12K camera (Starr et al. 2000) on the Palomar Observatory 48-inch telescope (P48). Images were processed by the IPAC image subtraction and discovery pipeline which subtracts off the background galaxy light with stacked pre-SN images and performs forced point-spread-function (PSF) photometry at the location of the SN (Masci et al. 2017). The photometry is then calibrated to the PTF photometric catalog (Ofek et al. 2012).

After discovery, photometric observations in the g', r' and i' filters were obtained with the SED Machine (SEDm; Blagorodnova et al. 2017, in prep.) mounted on the Palomar Observatory 60-inch telescope (P60). We utilized the Fremling Automated Pipeline (Fremling et al. 2016) to subtract galaxy light from the SEDm images using archival Sloan Digital Sky Survey (SDSS) images as a reference. This pipeline then performed forced-PSF photometry at the location of iPTF 16abc, which is calibrated to the SDSS catalog (Ahn et al. 2014).

[2] P48 observations of iPTF 16abc is reported in the $g_{\rm PTF}$ and $R_{\rm PTF}$ filters throughout, which are similar to the SDSS g' and r' filters, respectively (see Ofek et al. 2012 for details on PTF calibration). The correction from the $g_{\rm PTF}$ and $R_{\rm PTF}$ filters to SDSS g' and r' requires knowledge of the intrinsic source color (see Eqns. 1 and 2 in Ofek et al. 2012). The spectral diversity of SNe Ia in the days after explosion is poorly constrained, and as a result the color terms for iPTF 16abc at these epochs are unknown. We proceed by assuming $g_{\rm PTF}$ and $R_{\rm PTF}$ calibration is on the AB system, which strictly speaking is incorrect, but this does not fundamentally alter any of our conclusions.

Photometric observations in the *BVg'r'i'* filters were conducted by the Las Cambres Observatory (LCO) 1-m telescope network. PSF photometry was measured on these images using the `lcogtsnpipe` pipeline (Valenti et al. 2016). The *BV* magnitudes are calibrated to the Fourth USNO CCD Astrograph Catalog (Zacharias et al. 2013), and the *g'r'i'* magnitudes are calibrated to SDSS Data Release 6 (Adelman-McCarthy et al. 2008).

The *Swift* satellite observed iPTF 16abc on 14 epochs, beginning ∼15 d pre-maximum light through ∼22 d post maximum. The SN flux is measured via aperture photometry on Ultraviolet-Optical Telescope (UVOT) images via the usual procedures in `HEASoft`, including corrections for the coincident loss and aperture loss. The image counts are converted to physical fluxes using the latest calibration (Breeveld et al. 2011). There are no pre-SN UVOT images at the SN location in the *Swift* archive. Visual inspection of the UVOT images suggests negligible host-galaxy contamination in our UVOT flux measurements. No X-ray emission is detected from iPTF 16abc by the *Swift* X-ray Telescope (XRT).

The g-band discovery data and color curves of iPTF 16abc are illustrated in Figure 1. For convenience, magnitudes in *all* filters are in the AB system with a zero point of 3631 Jy. As previously noted the color terms necessary to convert the $g_{\rm PTF}$ and $R_{\rm PTF}$ to the AB system are unknown and assumed to be zero.

Spectroscopic observations of iPTF 16abc were taken with a variety of telescopes and instruments over multiple epochs spanning from a couple of days after explosion to two months after B-band maximum. An observing log is listed in Table 1. The spectra were reduced using standard routines in `IDL/Python`. The optical spectral evolution of iPTF 16abc is illustrated in Figure 2, which excludes high-resolution Very Large Telescope (VLT) spectra for clarity.

3. REDDENING, CLASSIFICATION AND HOST GALAXY

3.1. *Reddening*

A detailed study of the reddening towards iPTF 16abc is presented in a companion paper (Ferretti et al. 2017, submitted). Briefly, the foreground Galactic extinction toward iPTF 16abc is $E(B-V) = 0.0279$ mag (Schlafly & Finkbeiner 2011). The high-resolution spectra presented in Ferretti et al. (2017) show multiple absorption components for both the Ca II H+K and Na I D doublets. While the equivalent width (EW) of these lines is quite large, implying a large amount of extinction (e.g., Poznanski et al. 2012), Ferretti et al. compare the evolution of iPTF 16abc to the well-observed normal type Ia SN 2011fe and find evidence for only a small amount

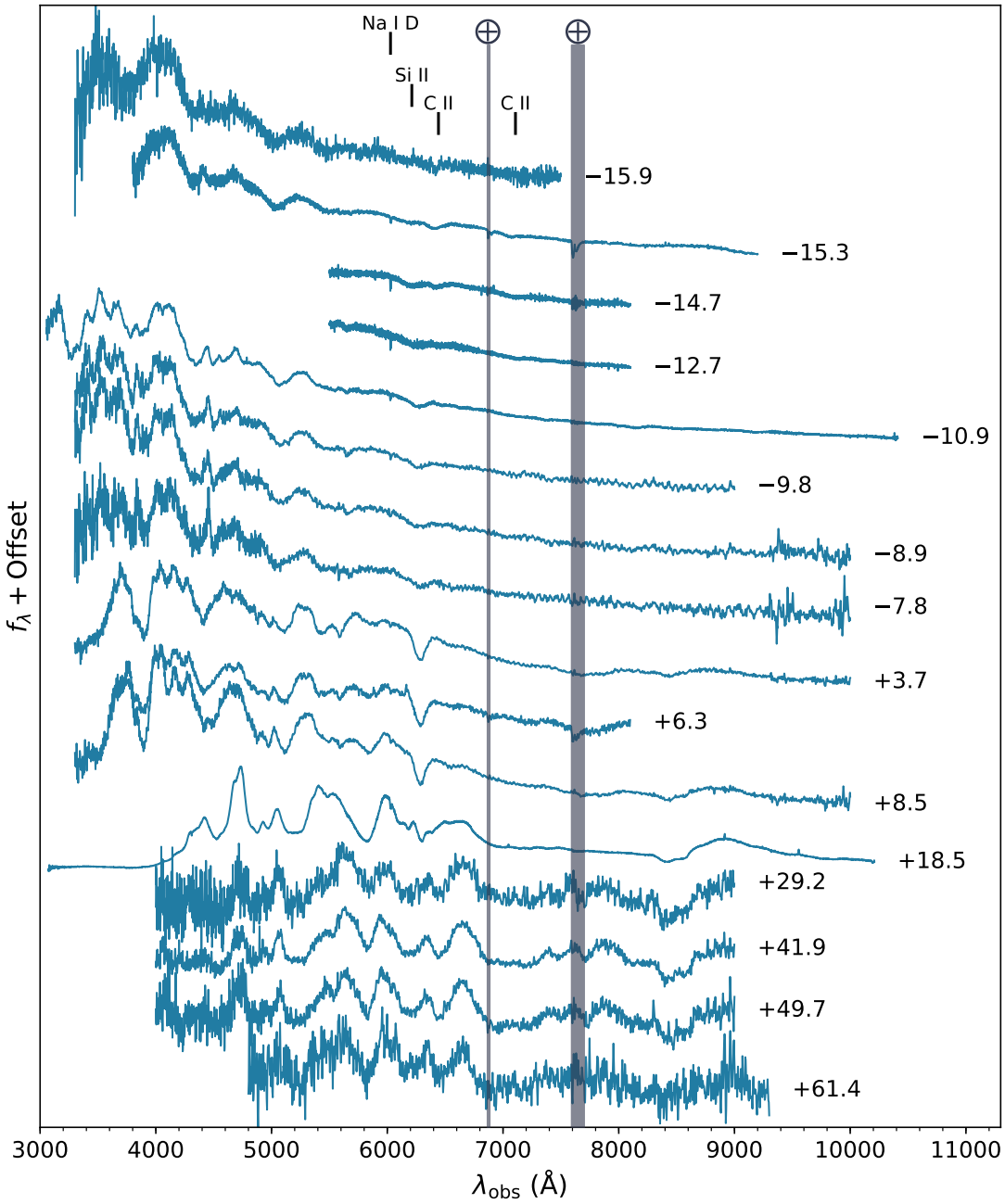

Figure 2. Observed spectral sequence of iPTF 16abc. The spectra are normalized by their median flux between 6,000 and 7,000 Å. The phase of each spectrum relative to $T_{B_{max}}$ is shown. Telluric absorption bands are grayed out. Line identifications are provided for the spectral features discussed in the text. For clarity, high-resolution spectra obtained with the VLT have been omitted (see Ferretti et al. 2017, submitted, for a detailed discussion of these spectra).

of extinction. The empirical relation between the EW of Na I D and extinction is known to have a large scatter, and thus, we instead adopt $E(B-V) = 0.05$ mag as the local extinction for iPTF 16abc (Ferretti et al. 2017). For the remainder of our analysis we therefore adopt a total, Galactic + host galaxy, line-of-sight extinction of $E(B-V) = 0.0779$ mag.

3.2. *Classification*

Using the Supernova Identification (SNID; Blondin & Tonry 2007) package, we find the low-resolution spectrum of iPTF 16abc at +18.8 d is best matched by normal SNe Ia. Several characteristic features of a SN Ia, such as Si II, S II, can be easily identified in the spectra of iPTF 16abc (Figure 2).

Table 1. Spectroscopic observations of iPTF 16abc

Observation MJD	SN phase	Telescope	Instrument	Range (Å)
57483.26	−15.9	DCT	DeVeny[1]	3301–7499
57483.88	−15.3	Gemini-North	GMOS[2]	3800–9200
57484.51	−14.7	Keck-II	DEIMOS[3]	5500–8099
57486.51	−12.7	Keck-II	DEIMOS[3]	5500–8099
57488.38	−10.9	Keck-I	LRIS[4]	3055–10411
57489.51	−9.8	LCOGT-2m	FLOYDS[5]	3301–8999
57490.40	−8.9	LCOGT-2m	FLOYDS[5]	3301–9999
57491.55	−7.8	LCOGT-2m	FLOYDS[5]	3300–9998
57492.20	−7.2	VLT	X-shooter[6]	3300–24550
57494.00	−5.4	VLT	UVES[7]	
57503.32	+3.7	LCOGT-2m	FLOYDS[5]	3300–9999
57506.00	+6.3	NOT	ALFOSC[8]	3602–8098
57508.27	+8.5	LCOGT-2m	FLOYDS[5]	3301–9999
57518.42	+18.5	Keck-I	LRIS[4]	3071–10208
57520.03	+20.0	VLT	X-shooter[6]	3300–24789
57529.40	+29.2	LCOGT-2m	FLOYDS[5]	4000–8998
57542.41	+41.9	LCOGT-2m	FLOYDS[5]	4000–8998
57550.40	+49.7	LCOGT-2m	FLOYDS[5]	4001–8999
57562.38	+61.4	LCOGT-2m	FLOYDS[5]	4800–9300

[1]The Deveny Spectrograph (Bida et al. 2014)

[2]The Gemini Multi-Object Spectrograph (Hook et al. 2004)

[3]DEep Imaging Multi-Object Spectrograph (Faber et al. 2003)

[4]Low-Resolution Imaging Spectrometer (Oke et al. 1995)

[5]FLOYDS https://lco.global/observatory/instruments/floyds

[6]X-shooter (Vernet et al. 2011)

[7]Ultraviolet and Visual Echelle Spectrograph (Dekker et al. 2000)

[8]The Andalucia Faint Object Spectrograph and Camera http://www.not.iac.es/instruments/alfosc

To determine the brightness and time of B-band maximum for iPTF 16abc, we fit the P60 light curves with the `sncosmo` software package.[3] This fit includes a SALT2 template (Guy et al. 2007) modified by the line-of-sight extinction curve (Fitzpatrick 1999) with $E(B-V)$ values from §3.1 and $R_V = 3.1$.

We determine the time of rest-frame B-band maximum to be $\mathrm{MJD}_{max} = 57499.54 \pm 0.23$, the coefficient of the zeroth principle component $x_0 = 0.0086 \pm 0.0003$, the coefficient of the first principle component $x_1 = 0.96 \pm 0.15$, and the color term $c = 0.033 \pm 0.029$. The best-fit model also gives an unreddened apparent peak magnitude of $m_B^* = 15.80 \pm 0.04$ mag in the SN rest frame.

For convenience, in the following sections, we define the best-fit value $\mathrm{MJD}_{max} = 57499.54$ as the time of B-band maximum, $T_{B_{\max}}$, which we also adopt as phase $t = 0$.

3.3. *Host Galaxy*

After establishing iPTF 16abc as a normal SN Ia, we use the latest calibration (Betoule et al. 2014) of the Phillips relation (Phillips 1993) using m_B^*, x_1 and c to derive a distance modulus $\mu = 34.88 \pm 0.10$ mag to the SN, provided that the host galaxy of iPTF 16abc has a stellar mass less than $10^{10} M_\odot$. We note that a more massive host galaxy would result in a larger inferred distance modulus that is nevertheless consistent within the uncertainties.

The location of iPTF 16abc is spatially coincident with a tidal tail of galaxy NGC 5221. Theureau et al. (2007) derived a distance modulus of 35.0 ± 0.4 mag to NGC 5221 from the Tully-Fisher relation, which is consistent with that of iPTF 16abc.

Separately, Courtois & Tully (2015) observe the 21-cm line in NGC 5221 and measure a redshift of 0.0234, which we adopt for the remaining analysis in this paper.

4. EARLY OBSERVATIONS

Here we consider our suite of early observations of iPTF 16abc, and compare our findings with SN 2011fe, a well-studied, nearby SN that was discovered shortly after explosion (Nugent et al. 2011; Bloom et al. 2012; Piro & Nakar 2014).

4.1. *Time of First Light from the Early Light Curve*

The time of first light for SNe is usually estimated by extrapolating early-phase light curves to determine when the SN is equal to 0. Assuming an ideal expanding fireball with constant temperature, Arnett (1982) derives that $f \propto t^2$, where f is the SN flux and t is the time since explosion. Despite the basic assumption of a constant temperature at early times, multiple studies have found that the early emission from type Ia SNe can be described as a power law in time, with power-law index consistent with 2, i.e. $f \propto t^2$ (e.g., (Conley et al. 2006; Hayden et al. 2010b; Ganeshalingam et al. 2011)).

[3] The `sncosmo` Python module is available at https://sncosmo.readthedocs.io/en/v1.5.x/.

As our observations include especially early observations of iPTF 16abc, there are upper limits ∼1 d prior to the discovery epoch, we model the early flux from iPTF 16abc as a power law, but allow the power-lax index to vary, as opposed to fixing it at 2, to account for potential variations in the photospheric temperature during expansion:

$$f(t) \begin{cases} = 0, \text{ when } t < t_0 \\ \propto (t - t_0)^{\alpha}, \text{ when } t > t_0 \end{cases} , \quad (1)$$

where t_0 is the time of first light, α is the power-law index, and t is measured in the rest-frame of the SN. To determine t_0 and α we fit the earliest observations of iPTF 16abc. Due to slight variations in the passbands, we fit the model to the relative flux measured in the $g_{\rm PTF}$-band, which is the only filter with observations prior to first light, a necessity for constraining t_0.

To determine the best fit parameters, we search a large grid over t_0, α and the proportionality constant, and minimize χ^2. The modeling results show that the SN flux rises approximately linearly between $t = -18$ d and $t = -14$ d. Figure 3 shows the best-fit result and the joint marginal distribution of t_0 and α. From the best-fit model we obtain $\alpha = 0.98 \pm^{0.16}_{0.14}$ and $t_0 = -17.91 \pm^{0.07}_{0.15}$ d, where the uncertainties represent the marginalized 95% confidence intervals. Our first detection of iPTF 16abc occurred ∼ 0.15 d after the SN first light. Figure 3 additionally shows g'-bands observations from P60 and LCO, where we have normalized the flux assuming that the g magnitudes from each instrument have the same zero-point. This assumption is incorrect (see §2), and, as expected, the residuals show a systematic offset between the $g_{\rm PTF}$-band and the g'-band. Nevertheless, if we ignore this systematic and fit all of the g-band observations simultaneous we obtain marginalized best-fit parameters that are consistent within the uncertainties with the $g_{\rm PTF}$-only values above. In the analysis that follows, the precise values of the best-fit parameters is not important. The critical finding here is that $\alpha \approx 1$ and $t_0 \approx -18$ d.

As previously noted, the early emission from most SNe Ia can be explained via a $f \propto t^2$ model, including SNe with extremely early observations like iPTF 16abc, such as SN 2011fe (Nugent et al. 2011). Thus, the near-linear rise in flux over the first few days after first light for iPTF 16abc is unusual. To our knowledge this behavior has only been observed in 2 other SNe (2013dy, 2014J; Zheng et al. 2013, 2014). Any model to explain the observations of iPTF 16abc must be able to account for this unusual behavior in the days after first light.

4.2. *Time of Explosion from the Photospheric Velocity*

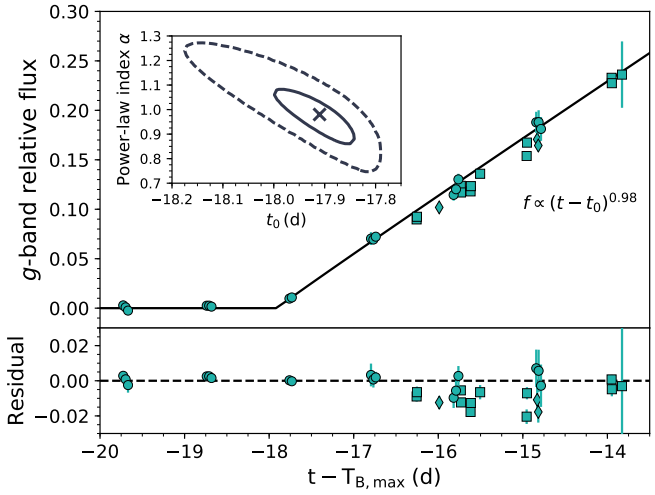

Figure 3. Best-fit power-law model to describe the early flux from iPTF 16abc in the $g_{\rm PTF}$-band. The model flux, adopting best-fit parameters $\alpha = 0.98$ and $t_0 = -17.94$ d, is shown as a solid black line in the top panel. The lower panel shows the model residuals, and the symbols are the same as in Figure 1. The model is fit to just the $g_{\rm PTF}$-band observations to avoid systematic difference between the filters (see the text for further details). The joint distribution of t_0 and α is illustrated in the inset of the upper panel. The solid and dashed contours represent the 68% and 99.7% confidence levels.

As previously noted, t_0 does not correspond to the time of explosion, $t_{\rm exp}$, for type Ia SNe as the SN may experience a dark phase following shock breakout before radioactive energy can diffuse to the photosphere. Piro & Nakar (2014) instead suggest that measurements of the photospheric velocity be used to determine $t_{\rm exp}$ given that the ejecta begin expanding from the moment of explosion. Assuming a constant opacity in the ejecta, Piro & Nakar find that the photospheric velocity evolves as $v_{ph} \propto (t - t_{\rm exp})^{-0.22}$. Numerical experiments by Piro & Morozova (2016) find that the consatnt-opacity assumption strongly depends on the amount of ^{56}Ni mixing in the SN ejecta (for a more detailed discussion of ^{56}Ni mixing see §5.4). As a result, the adoption of a $t^{-0.22}$ power-law model may not be valid for all SNe Ia. Nevertheless, we proceed on the assumption that iPTF 16abc experienced strong ^{56}Ni mixing, corresponding to the models that are best approximated as a $t^{-0.22}$ power law. We do this in part to compare with previous studies, though we caution that our derived value for t_{exp} is subject to uncertainties related to ejecta mixing.

While the photospheric velocity is not easy to measure, line velocities of Si II or Ca II can be used as a proxy (Piro & Nakar 2014; Shappee et al. 2016b). In the case of iPTF 16abc, the Ca II IR triplet is very weak, likely due to high temperatures in the ejecta. Thus, we

determine the photospheric velocity from the Si II λ6355 line. Visual inspection shows no sign of multi-velocity components of Si II, and that the C II λ6580 line overlaps the red wing of the Si II line (see Figures 2 and 5). Consequently, we model the observed spectra between 5,900 and 6,500 Å (rest-frame) as the combination of two gaussian kernels plus a linear baseline, which accounts for Si II, C II and the continuum, respectively. The expansion velocity of Si II is measured by the central wavelength of the Si II Gaussian kernel.

We fit the measured velocities of Si II λ6355 to the $v \propto (t - t_{exp})^{-0.22}$ model by minimizing the χ^2 value and find the best-fit explosion time relative to $T_{B,\rm max}$ in the SN rest frame to be $t_{exp} = -17.45\ ^{+0.14}_{-0.16}$ d, where the uncertainties represent the 95% confidence interval (Figure 4). Following the analysis in Piro & Nakar (2014), we additionally alter the power-law index to -0.20 and -0.24 to examine the sensitivety of the result on the assumed power-law index. We find that this variation in the power-law index results in inferred explosion times that vary by $\approx$1 d (Figure 4). Given the analytical approximation that $v \propto t^{-0.22}$, we adopt $t_{exp} = -17.5 \pm 0.5$ d, where the uncertainty reflects possible variations in the power-lax index (see Piro & Nakar 2014).

Comparing our estimates for t_{exp} and t_0 (left panel of Figure 4), we find that $t_0 \lessapprox t_{exp}$. Since physical causality requires $t_{exp} < t_0$, we draw the qualitative conclusion that $t_0 \simeq t_{exp}$, which is consistent to within the uncertainties. Again, we caution that this derivation of $t_{\rm exp}$ relies on the assumption $v \propto t^{-0.22}$, which may not be valid for all SNe Ia.

4.3. *Strong and Short-Lived Carbon Features*

The early spectra of iPTF 16abc exhibit unusually strong absorption due to C II $\lambda\lambda$6580, 7234. We highlight the evolution of these spectral features in Figure 5. From these spectra we see that C II λ6580 is as strong as Si II λ6355 at $t \approx -16$ d. The strength of the C II lines declines with time to the point where they are no longer detectible more than 1 wk after explosion.

Similar to our analysis of the Si II λ6355 line, we can measure velocities and pseudo-equivalent widths (pEWs) of C II $\lambda\lambda$6580, 7234. We compare the velocity evolution of the C II lines to Si II in the right panel of Figure 4, which also shows the pEW evolution of these lines. These measurements confirm the qualitative analysis from Figure 5: namely, the pEW of C II λ6580 is comparable to that of Si II λ6355 at $t \approx -16$ d and the pEW of C II decreases until the feature is no longer detectable around $t = -10$ d.

The detection of C II in SNe Ia spectra is relatively rare as it requires both unburned carbon, which is likely only present in the outermost layers of the ejecta, and non-local thermal equilibrium effects in order to excite the ionized carbon (e.g., Thomas et al. 2007). Spectra obtained around or after $T_{B_{\rm max}}$ rarely show C II as the photosphere has receded from the outermost ejecta, while pre-max spectra show evidence for C II in $\sim$1/4 of all normal SNe Ia (e.g., Parrent et al. 2011; Silverman & Filippenko 2012; Thomas et al. 2011), but the signatures are typically weak. While we caution that the sample of normal SNe Ia with spectra taken within a few days of explosion is small, SN 2013dy is the only other object known to have strong C II features like iPTF 16abc (Zheng et al. 2013). As a counterexample, SN 2011fe only exhibited weak C II features in its first spectra (Parrent et al. 2012). Thus, models of iPTF 16abc must explain the anomalously strong C II absorption observed shortly after explosion.

4.4. *Blue Optical Colors Shortly After Explosion*

Multiband observations of iPTF 16abc began $\sim$1.5 d after discovery, which allows us to trace its color evolution starting $\sim$1.7 d after t_0. In Figure 6 we compare the $(B-V)_0$ color evolution of iPTF 16abc and SN 2011fe, where the observations of SN 2011fe are taken from Zhang et al. (2016). For both SN the colors have been corrected for the total inferred redenning along the line of sight. Interestingly, iPTF 16abc has a nearly flat color evolution up to 10 d before $T_{B,\rm max}$, while SN 2011fe exhibits red colors initially before eventually becoming as blue as iPTF 16abc.

Roughly 16 d prior to B-band maximum, the $(B-V)_0$ color of iPTF 16abc is $\sim$0.5 mag bluer than SN 2011fe. Like iPTF 16abc, SN 2012cg (Marion et al. 2016) and SN 2017cbv (Hosseinzadeh et al. 2017) exhibit $(B-V)_0$ colors that are significantly bluer than SN 2011fe at very early epochs. While there are many factors that contribute to the early optical colors of SNe Ia (see §5 below), early blue colors are often interpreted as a hallmark of interaction between the SN ejecta and a binary companion. Nevertheless, it is interesting to note that despite the blue optical colors the UV $-$ optical colors of iPTF 16abc, SN 2012cg, and SN 2017cbv are significantly redder at these early epochs than the UV $-$ optical colors of iPTF 14atg (Cao et al. 2015), the most likely candidate for an ejecta-companion interaction SN.

5. DISCUSSION

Relative to the nearby, normal SN 2011fe, we have identified several unusual properties in the early observations of iPTF 16abc, including: (i) a near-linear photometric rise in the days after explosion, (ii) the lack

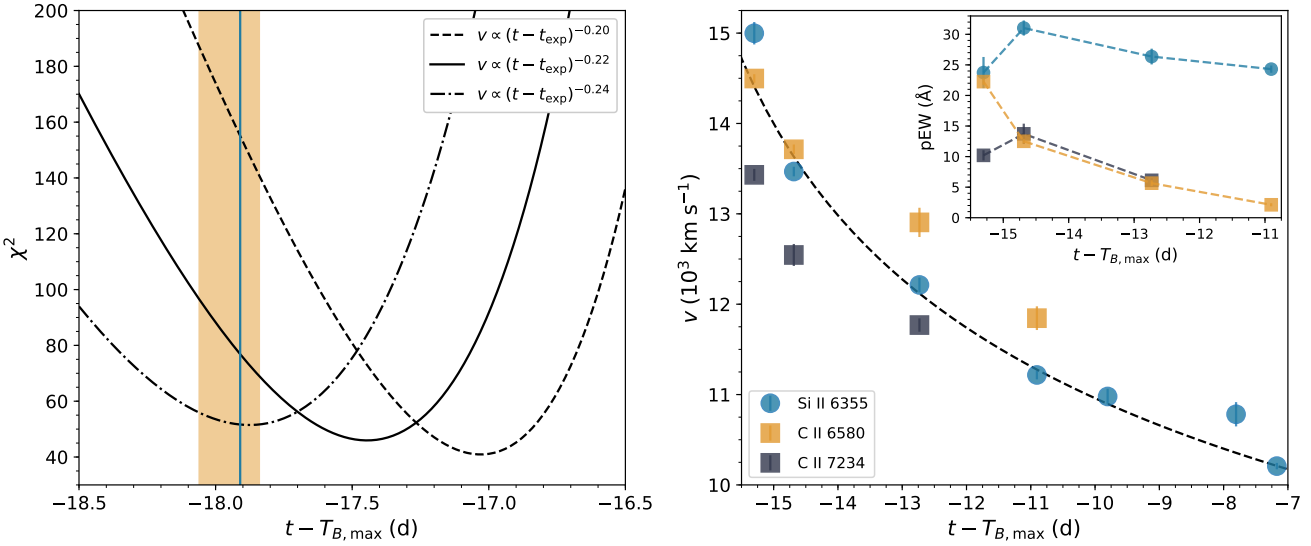

Figure 4. Constraints on t_{exp} from fitting the velocity evolution of Si II. *Left panel:* the dashed, solid and dash-dotted curves show χ^2 for fitting power laws with indices -0.20, -0.22 and -0.24, respectively. The blue vertical line and the orange shaded region indicate t_0 and its 95% confidence interval from Section 4.1, respectively. *Right panel:* Observed Si II λ6355 velocities (blue circles) and the best-fit power-law model with an index of -0.22 (dashed line). Additionally the measured velocites of C II $\lambda\lambda$6580, 7234 are shown. *Right inset*: Evolution of the pseudo-equivalent width of Si II λ6355, and C II $\lambda\lambda$6580, 7234 in the week following explosion.

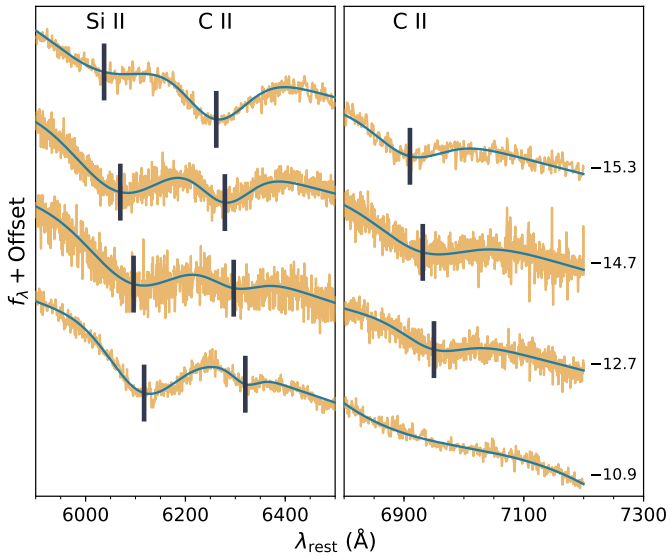

Figure 5. Evolution of the C II features observed in the early spectra of iPTF 16abc. The raw spectra are shown in orange, while the solid blue lines show the best-fit models including gaussian components for each line and a linear component for the continuum (see text for further details). The dark grey vertical lines show the measured line centers, indicating the decline in the photosphere velocity in the ∼wk after explosion (note that C II λ7234 is not detected in the -10.9 d spectrum). The phase of each spectrum relative to $T_{B,max}$ is shown to the right of each spectrum.

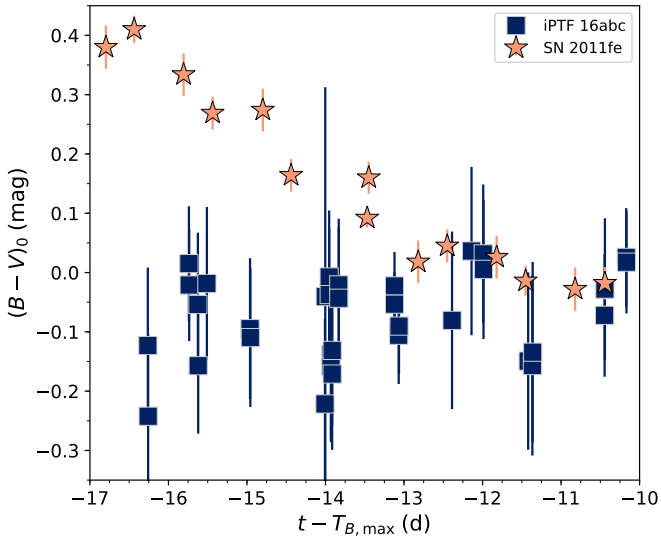

Figure 6. $(B-V)_0$ color evolution of iPTF 16abc (shown as squares) compared to SN 2011fe (shown as stars). The B and V photometry are calibrated on the Vega system, and have been corrected for extinction. The data for SN 2011fe are from Zhang et al. (2016).

of a dark phase typical of most SNe Ia, and (iii) the presence of strong C II absorption. While most SNe Ia are powered purely by radioactive decay, the observed radiation shortly after explosion can also include contributions from SN shock cooling or the collision of the SN ejecta with a non-degenerate companion. Here we consider those scenarios as a possible explanation for the early behavior of iPTF 16abc.

5.1. *SN Shock Cooling*

The shock breakout of a SN Ia lasts for a fraction of a second due to compact size of the exploding star. Emission from the subsequent cooling phase may last for several days, however (e.g., Piro et al. 2010). Following the analysis of Bloom et al. (2012) for SN 2011fe, we compare the early-phase $g_{\rm PTF}$ light curve of iPTF 16abc with two shock cooling models (Rabinak & Waxman 2011; Piro et al. 2010). From this analysis, we constrain the iPTF 16abc progenitor radius to be $< 1 R_\odot$. Our observations of iPTF 16abc cannot place tight constraints on the size of SNe Ia progenitors. Indeed, for a typical WD radius, such as that inferred for SN 2011fe ($\lesssim 0.02$–$0.04\,R_\odot$; Bloom et al. 2012; Piro & Nakar 2014), the expected emission from shock cooling is $\sim$2 mag fainter than the P48 $g_{\rm PTF}$ detection limit. Thus, we conclude that shock cooling does not contribute to the early emission from iPTF 16abc.

5.2. *SN-Companion collision*

The detection of excess emission due to the collision of the SN ejecta with a non-degenerate companion requires a favorable orbital alignment relative to the line of sight. Thus, from geometric considerations alone the probability of detecting ejecta-companion interaction is low, $\sim$10%. Kasen (2010) calculates that the collision of SN ejecta with a companion generates thermal emission with a spectrum that peaks in the UV. The resulting g-band emission is expected to be weak.

To examine the possibility of a SN-companion signature in the early light curve of iPTF 16abc, we employ the Kasen (2010) model and assume canonical values for the ejecta mass, $1.4\,M_\odot$, expansion velocity, $10^4\,{\rm km\,s^{-1}}$, and a constant opacity, $0.2\,{\rm cm^2\,g^{-1}}$. We calculate the expected $g_{\rm PTF}$ brightness of an ejecta-companion collision at the distance of iPTF 16abc behind a total reddening of $E(B-V) = 0.0779$ mag using the parameterized equations in Brown et al. (2012). If we assume the binary is aligned with the optimal orientation relative to the line of sight, a binary separation of $a \approx 2\times10^{13}$ cm is needed to explain the initial detection of iPTF 16abc, as shown in Figure 7. This model does not, however, match the $g_{\rm PTF}$ evolution for $t > t_0 + 1$ d (though it is possible that the SN photosphere dominates the companion-interaction signature at this phase). Furthermore, this model significantly overpredicts the observed flux in the *Swift*/$UVW1$ filter $\sim$3.1 d after t_0. As such, we do not favor such a model as the explanation for the early emission from iPTF 16abc.

Figure 7 additionally shows that a companion at $a = 10^{14}$ cm provides a good match to the observations $\sim$1–3 d after t_0 if $t_{\rm exp} \approx t_0 + 0.3$ d. Like the $a = 2\times10^{13}$ cm model, this model significantly overpredicts the observed UV flux from iPTF 16abc. Additionally, this model cannot account for the brightness of iPTF 16abc at the epoch of discovery. The challenges associated with each of the previous two models lead us to conclude that the early evolution of iPTF 16abc cannot be explained via the interaction of the SN ejecta with a red-giant companion.[4] We cannot, however, exclude the presence of a red-giant companion as our calculations have assumed that the binary is aligned with the optimal geometry relative to the line of sight. If the geometry is not favorable, then it is possible that signatures from interaction with a companion are not visible.

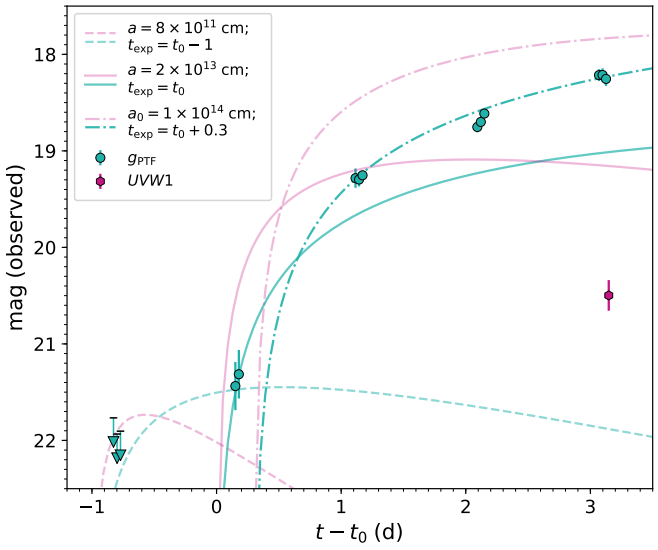

Figure 7. Comparison of SN ejecta-companion interaction models with early observations of iPTF 16abc. $g_{\rm PTF}$ observations (green) detections and 3σ upper limits are shown as circles and downward arrows, respectively. The initial *Swift*/$UVW1$ observation (magenta) is shown as a hexagon. The dashed, solid, and dash-dot lines show the expected flux for various companion interaction models in the $g_{\rm PTF}$ (green) and $UVW1$ (magenta) filters. The models have been adjusted to account for the distance and redenning towards iPTF 16abc. Each model features a different companion semi-major axis, a, and time of explosion, $t_{\rm exp}$, as labeled in the figure legend. While models with $a \gtrsim 10^{13}$ cm can explain the early $g_{\rm PTF}$ emission, they greatly overpredict the flux in the UV. If the time of explosion is $\sim$1 d prior to t_0, then models with $a \approx 10^{12}$ cm can explain the initial detection iPTF 16abc, but they fail to replicate the $\sim$2 mag rise in the $\sim$24 hr after explosion. Thus, SN ejecta-companion interaction models fail to uniquely explain the early flux from iPTF 16abc.

[4] The Kasen (2010) model assumes Roche-lobe overflow, meaning that $a > 10^{13}$ cm implies a companion with $R_* \gtrsim 100\,R_\odot$.

Finally, we examine the minimum binary separation capable of explaining the observed brightness at the epoch of discovery. Figure 7 shows that models with $a \approx 8 \times 10^{11}$ cm peak at ∼21.5 mag in the $g_{\rm PTF}$-band, provided that $t_{\rm exp} \approx t_0 - 1$ d. To explain just the epoch of discovery, models with larger a would require even earlier explosion times, which is not compatible with our non-detections the night before discovery, while models with smaller a are not bright enough. While it is otherwise compatible with the observations, we do not favor the $a \approx 8 \times 10^{11}$ cm model as the explanation for the early flux from iPTF 16abc because it does not explain the 2 mag rise in the ∼24 hr after discovery.

5.3. *Interaction with Diffuse Material*

Here we consider a model that has not, as of yet, been discussed in the context of iPTF 16abc. To model SN 2011fe, Dessart et al. (2014) recently examined pulsational delayed-detonation (PDD) models as an explanation for some SNe Ia. Briefly, PDD models differ from "standard" delayed detonation (DD) models in that the initial deflagration causes the WD to expand resulting in the release of some unbound material. As the bound material contracts, eventually a subsequent detonation occurs.[5] An important consequence of this sequence for PDD models is that they naturally produce material that avoids burning, unlike DD models that typically leave no unburnt material. This enables the presence of significantly more carbon in the outer layers of the SN ejecta (Dessart et al. 2014).

When comparing observations of SN 2011fe to their DD models, Dessart et al. (2014) find that the models are universally too faint and red at early times, ∼24-48 hr after explosion. Instead, Dessart et al. (2014) find that PDD models provide a better match to observations. Briefly, the diffuse material surrounding the WD heats the outer layers of the SN ejecta leading to a steeper more luminous rise, with bluer colors in the few days after explosion. Importantly, the PDD models are nearly indistinguishable from DD models around and post peak.

Qualitatively, the PDD models provide a better match to the observations of iPTF 16abc than DD models. In particular, PDD models provide higher luminosities and faster rise times in the days after explosion, a more rapid evolution towards blue optical colors, and the formation of strong C II lines that gradually disappear in the ∼week after explosion. Quantitatively, there are still some short comings of the models presented in Dessart et al. (2014). In particular, the power-law index for the g-band rise is $\alpha \approx 3$ for each of the PDD models, which is significantly more steep than $\alpha = 0.98$, which we measure for iPTF 16abc. The optical colors for iPTF 16abc are blue from our first epoch ∼1.7 d after explosion and remain approximately constant in the 10 d after explosion, whereas the PDD models in Dessart et al. (2014) either exhibit distinct color evolution (i.e. are not constant) or are too red in the first few days after explosion. Nevertheless, the PDD models presented in Dessart et al. (2014) provide several attractive explanations for the unusual features in the early behavior of iPTF 16abc, and it may be possible that small adjustments to the model (e.g., additional mixing of the radioactive material, adjustments in the explosion energy, etc.) can better match iPTF 16abc.

[5] Dessart et al. (2014) note that the deflagration and detonation in their PDD models are artificially triggered.

5.4. *Strong ^{56}Ni Mixing as an Explanation for iPTF 16abc*

Having examined other possibilities we now consider whether the unusual properties of iPTF 16abc can be explained simply by invoking strong mixing in the SN ejecta. As previously mentioned, strong mixing can lead to a short dark phase. Here we additionally examine whether strong mixing can explain the rapid, near-linear rise in the light curve.

In Figure 8 we compare model calculations from Piro & Morozova (2016) to the observed photometry of iPTF 16abc. The Piro & Morozova models employ a piston driven explosion to explode a single WD progenitor model. As the piston explosion does not result in any nucleosynthesis, the distribution of ^{56}Ni in the ejecta must be prescribed by hand, which enables the study of the effects of mixing on the resulting SN emission. Each model employs a fixed $0.5\,M_\odot$ of ^{56}Ni that has been distributed throughout the ejecta via boxcar averaging (see their Figure 1). The resulting light curves are synthesized using the SuperNova Explosion Code (SNEC; Morozova et al. 2015), as shown in Figure 8. Broadly speaking, the results can be summarized as follows: SN with strong mixing exhibit a rapid almost linear rise and quickly develop blue colors, whereas models where the ^{56}Ni is confined to the innermost layers of the ejecta remain very faint for days after explosion while exhibiting relatively red optical colors during this period. The fast rise and blue color of iPTF 16abc are qualitatively consistent with the strong mixing models from Piro & Morozova (2016), as shown in Figure 8. In fact, if we adopt $t_{\rm exp} = t_0 - 0.45$ d, we find that the model with the strongest mixing (orange line in Figure 8 provides an excellent match to the g-band observations.

While the models from Piro & Morozova (2016) provide a good match to the optical photometric evolution of iPTF 16abc, they consistently overpredict the flux in the UV. The models shown in Figure 8 also overpredict the photospheric velocity of iPTF 16abc by ∼2–3,000 km s^{-1}. These discrepancies may be accounted for following an improved treatment of line-blanketing and a reduction in the model explosion energy, respectively. Future modeling efforts may improve the match between the simulations and observations for iPTF 16abc.

Both the PDD models and ejecta-mixing models show discrepancies with some of the early observations of iPTF 16abc. Nevertheless, we conclude that one, or both, of these scenarios, which feature qualitatively similar predictions, is the most likely explanation for iPTF 16abc.

5.5. *The Emerging Sample of Young SNe Ia*

The proliferation of high-cadence, time-domain surveys has led to several SNe Ia being discovered within $\lesssim$2 d of first light in the past ∼decade. Observations probing the early evolution of these SNe allows us to place unique constraints on their progenitor systems and the corresponding explosion physics. This has revealed diversity in the earliest epochs after explosion and that commonly used SNe Ia templates do not match observations (e.g., Foley et al. 2012).

In §5 we compared our early observations of iPTF 16abc to SN 2011fe, which has the most comprehensive observations of the young SNe Ia sample. Given its normal spectroscopic and photometric evolution, SN 2011fe has been adopted as a standard for the early evolution of SNe Ia in many studies. While a detailed quantitative analysis is beyond the scope of this study, a qualitative examination of very young SNe Ia that otherwise exhibit normal spectra and evolution at and post-peak[6] reveals considerable diversity. In other words, at early times SN 2011fe may not be the norm.

For SN 2011fe the initial rise is well described by a t^2 power law, the $(B-V)_0$ colors evolve from the red to the blue in the ∼week after explosion, and the C II present in the initial spectra is weak (Nugent et al. 2011; Zhang et al. 2016; Parrent et al. 2012). In contrast, iPTF 16abc exhibits a near linear rise in flux, the $(B-V)_0$ colors are blue and roughly constant, and the C II absorption is strong. Examining just these 3 qualitative features, SN 2009ig is well matched to SN 2011fe (Foley et al. 2012), while SN 2013dy (Zheng et al. 2013), SN 2017cbv (Hosseinzadeh et al. 2017), and iPTF 16abc

[6] This definition excludes iPTF 14atg, which was shown to be subluminous with SN 2002es-like spectra (Cao et al. 2015).

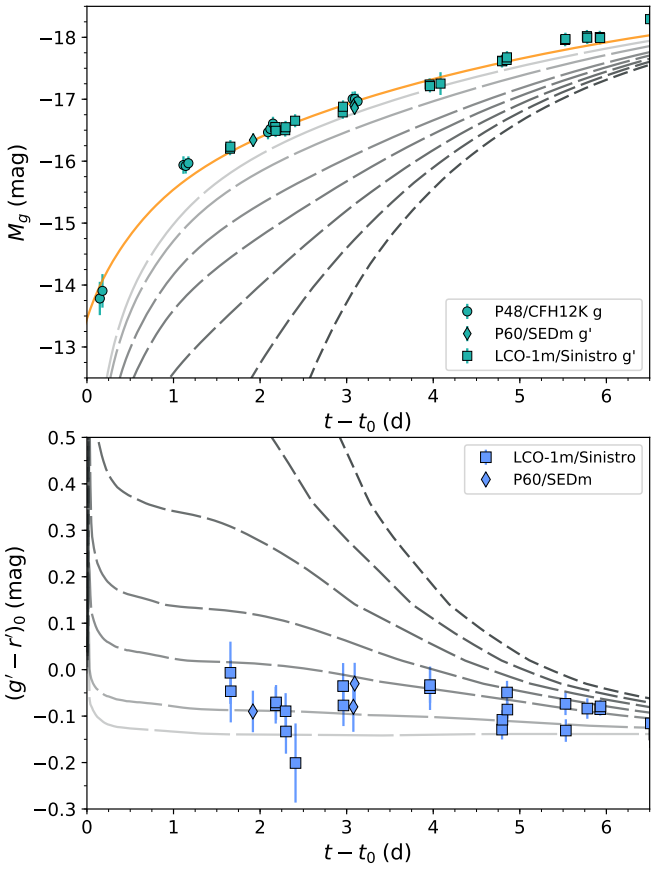

Figure 8. Photometric comparison of iPTF 16abc and the theoretical models of Piro & Morozova (2016). The amount of ^{56}Ni mixing in the SN ejecta increases from the short-dash, dark lines to the long-dash, light lines. *Top*: M_g vs. time, where the observed g-band magnitudes have been corrected to M_g using the distance modulus to iPTF 16abc (§3.3) and the total line-of-site reddening ($E(B-V) = 0.078$ mag; Ferretti et al. 2017, submitted). The orange solid line shows the model with the most ^{56}Ni mixing shifted to an explosion time of $t_0 - 0.4$ d. This model provides a good match to the data. *Bottom*: $(g'-r')_0$ vs. time. The observed colors have been corrected for reddening.

all bear a striking resemblance. SN 2012cg, on the other hand, is intermediate to these two groups with weak C II and a relatively shallow early rise, like SN 2011fe, but blue $(B-V)_0$ colors, like iPTF 16abc (Silverman et al. 2012; Marion et al. 2016). SN 2014J is intermediate in the other direction in that it exhibits a near linear rise (Zheng et al. 2014; Goobar et al. 2015), but the color evolution is very similar to SN 2011fe (Amanullah et al. 2014).[7] That these early observations cannot be eas-

[7] C II is not detected in the spectra of SN 2014J (Goobar et al. 2014; Zheng et al. 2014), though the earliest spectra of SN 2014J were obtained at a much later phase than the other SNe discussed here. Marion et al. (2015) find evidence for C I in the NIR spec-

ily separated into two distinct groups suggests that it is unlikely that a single physical mechanism drives the diversity of SNe Ia at early times.

In the case of SN 2012cg and SN 2017cbv it has been argued that the early blue optical colors are indicative of interaction between the SN ejecta and a binary companion (Marion et al. 2016; Hosseinzadeh et al. 2017). SN 2017cbv is particularly remarkable in that the observations presented in Hosseinzadeh et al. (2017) show a clearly resolved bump in the U, B, and g' bands in the $\sim$5 d after explosion. In Hosseinzadeh et al. it is found that the bump can be explained via the combination of ejecta-companion interaction and the normal evolution of a SN Ia. A challenge for this model, similar to iPTF 16abc (see §5.2), is that it significantly overpredicts the UV brightness of the SN compared to what is observed. Indeed, in the case of SNe 2012cg, 2017cbv, and iPTF 16abc the UV - optical colors are significantly redder than those observed in iPTF 14atg. It is argued in Hosseinzadeh et al. (2017) that several model assumptions, including: (i) ideal blackbody emission, (ii) a constant opacity, (iii) a simple power-law density profile for the ejecta, and (iv) spherical symmetry, may be incorrect, which could reconcile the discrepancy with the UV observations. Above, we argued for circumstellar interaction and strong ^{56}Ni mixing as a possible explanation for iPTF 16abc, and indeed Hosseinzadeh et al. (2017) consider these possibilities for SN 2017cbv as well. Seperately, several arguments against companion interaction for SN 2012cg are presented in Shappee et al. (2016a).

Ultimately, there are arguments in favor of and against each of the possibilties to explain the early emission from SNe Ia. Moving forward, more detailed models and simulations are needed to properly explain the observed diversity. No matter the correct explanation for the early behavior of SNe 2013dy, 2017cbv, and iPTF 16abc, the strong similarities between these events suggests they reflect a common physical origin.

6. CONCLUSION

We have presented observations of the extraordinarily early discovery of the normal Type Ia supernova iPTF 16abc. Our fast-response follow-up campaign allowed us to draw the following conclusions:

- Extrapolation of the early light curve shows that the initial detection of iPTF 16abc occurred only $\sim$0.2 d after the time of first light.
- The early emission from iPTF 16abc is powered solely by radioactive ^{56}Ni decay. We find no evidence for detectable signatures of SN shock cooling or the collision of the SN ejecta with a non-degnerate binary companion.
- The velocity evolution of the SN ejecta shows that the time of explosion is approximately equal to the time of first light. This constitutes the first major piece of evidence that ^{56}Ni is strongly mixed into the outer layers of the supernova ejecta.
- The strong and short-lived carbon features seen in the earliest spectra of iPTF 16abc can only be explained if there is incomplete burning during the explosion and there is a non-thermal radiation source in the outermost layers of the ejecta to excite the ionized carbon. ^{56}Ni decay is the likely source of the non-thermal emission, providing another piece of evidence for strong mixing in the ejecta of iPTF 16abc.
- Finally, we show that the early light curve evolution and colors of iPTF 16abc are well matched by the theoretical models of Piro & Morozova (2016) that include significant mixing of ^{56}Ni into the outer layers of the SN ejecta.

Taken together, these observations all indicate that the nucleosynthetic products from the explosion are well mixed throughout the SN ejecta. There are elements of the PDD models from Dessart et al. (2014) that are attractive for explaining iPTF 16abc, in particular, the strong C II absorption seen at early times. In the future, it would be useful to investigate PDD models that incorporate strong ^{56}Ni mixing to see if they better replicate the observations of iPTF 16abc.

Extremely early observations of young SNe provide a "smoking gun" to probe the mixing level in the ejecta, which, in turn, is a result of the explosion mechanism. Wide-field, high-cadence surveys, such as the Zwicky Transient Facility (Bellm 2016) and ATLAS (Tonry 2011, 2013), will discover a large number of very young supernovae over the next few years. These surveys will generate large observational samples that probe SNe in the hours after explosion. While the sample of extremely young SNe Ia will grow by more than an order of magnitude, the detection of shock breakout cooling and ejecta-companion interaction will prove challenging. Given the diminutive size of WDs, the thermal emission following shock breakout can only be detected to $\sim$ 10 Mpc on 1-m class telescopes. Furthermore, only $\sim$10% of single-degenerate progenitors are expected to give rise to detectable emission following the collision of the SN

tra of SN 2014J, but this detection cannot constrain the relative strength of C II and Si II shortly after explosion.

ejecta with the binary companion (Kasen 2010). Despite these limitations, this study of iPTF 16abc shows that the early detection of SNe Ia can constrain the explosion physics by probing the amount of mixing in the SN ejecta. Moving forward, a large sample of such objects will enable strict constraints on the proposed explosion mechanisms for type Ia SNe.

Finally, we close by emphasizing the importance of fast-response photometric and spectroscopic follow-up campaigns. Without the early recognition of the youth of this SN and the associated follow-up, much of the analysis presented herein would not have been possible. The ability to trigger such observations is essential to improve our understanding of the physics of SNe Ia.

We are deeply grateful to R. C. Thomas for induldging a slew of questions regarding C II in SNe. Similarly, it is our pleasure to buy a beer for R. Amanullah and U. Feindt for discussions regarding SALT2.

Much of the analysis presented herein would not have been possible without the help of several observers. We thank M. West for taking the first spectrum of iPTF 16abc as a ToO on the DCT. We also thank the Gemini service observers for executing our ToO observations. Additionally, J. Cohen, N. Suzuki, V. Ravi, R. Walters, A. Ho, and L. Yan helped obtain data for this paper.

AAM is funded by the Large Synoptic Survey Telescope Corporation in support of the Data Science Fellowship Program. YC thanks support from a postdoc fellowship in the eScience institute, University of Washington.

DAH, CM, and GH are supported by NSF-1313484. Support for IA was provided by NASA through the Einstein Fellowship Program, grant PF6-170148.

The Intermediate Palomar Transient Factory project is a scientific collaboration among the California Institute of Technology, Los Alamos National Laboratory, the University of Wisconsin, Milwaukee, the Oskar Klein Center, the Weizmann Institute of Science, the TANGO Program of the University System of Taiwan, and the Kavli Institute for the Physics and Mathematics of the Universe. This work was supported by the GROWTH project funded by the National Science Foundation under Grant No 1545949. Part of this research was carried out at the Jet Propulsion Laboratory, California Institute of Technology, under a contract with the NASA. This work makes use of observations from the LCO network.

APPENDIX

A. PHOTOMETRIC LIGHT CURVES

The full photometric light curves of iPTF 16abc are shown in Figure 9.

REFERENCES

Adelman-McCarthy, J. K., Agüeros, M. A., Allam, S. S., et al. 2008, ApJS, 175, 297

Ahn, C. P., Alexandroff, R., Allende Prieto, C., et al. 2014, ApJS, 211, 17

Amanullah, R., Goobar, A., Johansson, J., et al. 2014, ApJL, 788, L21

Arnett, W. D. 1982, ApJ, 253, 785

Bellm, E. C. 2016, PASP, 128, 084501

Betoule, M., Kessler, R., Guy, J., et al. 2014, A&A, 568, A22

Bianco, F. B., Howell, D. A., Sullivan, M., et al. 2011, ApJ, 741, 20

Bida, T. A., Dunham, E. W., Massey, P., & Roe, H. G. 2014, in Proc. SPIE, Vol. 9147, Ground-based and Airborne Instrumentation for Astronomy V, 91472N

Blondin, S., & Tonry, J. L. 2007, ApJ, 666, 1024

Bloom, J. S., Kasen, D., Shen, K. J., et al. 2012, ApJL, 744, L17

Breeveld, A. A., Landsman, W., Holland, S. T., et al. 2011, in American Institute of Physics Conference Series, Vol. 1358, American Institute of Physics Conference Series, ed. J. E. McEnery, J. L. Racusin, & N. Gehrels, 373–376

Brown, P. J., Dawson, K. S., Harris, D. W., et al. 2012, ApJ, 749, 18

Cao, Y., Kulkarni, S. R., Howell, D. A., et al. 2015, Nature, 521, 328

Cenko, S. B., Cao, Y., Kasliwal, M., et al. 2016, The Astronomer's Telegram, 8909

Conley, A., Howell, D. A., Howes, A., et al. 2006, AJ, 132, 1707

Courtois, H. M., & Tully, R. B. 2015, MNRAS, 447, 1531

Dekker, H., D'Odorico, S., Kaufer, A., Delabre, B., & Kotzlowski, H. 2000, in Proc. SPIE, Vol. 4008, Optical and IR Telescope Instrumentation and Detectors, ed. M. Iye & A. F. Moorwood, 534–545

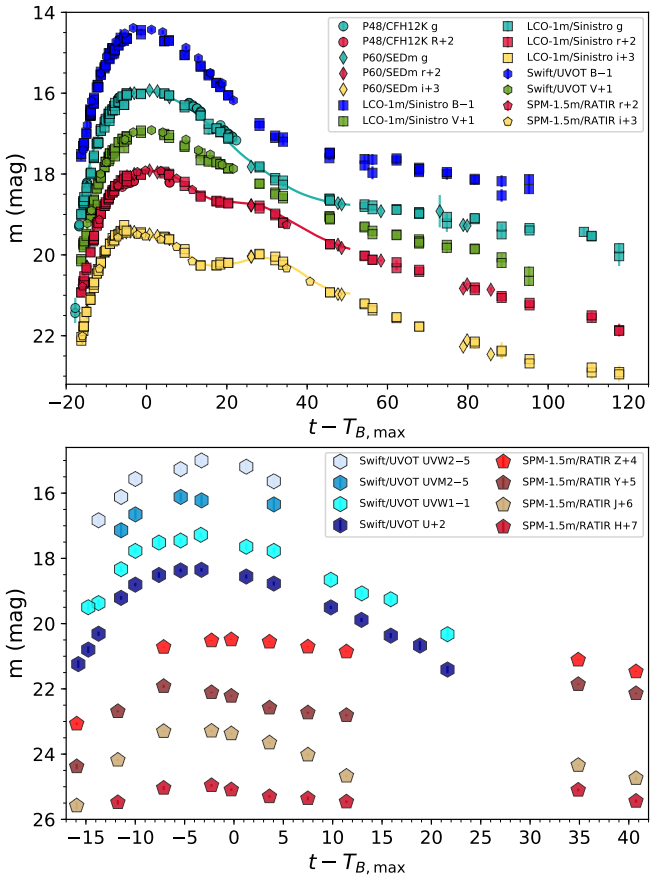

Figure 9. UV, optical, and NIR light curves for iPTF 16abc. *Top*: *BVgri* light curves from the P48, P60, and LCO-1m telescopes. The solid lines represent the best-fit model from SALT2 (see 3.2). *Bottom*: UV and NIR light curves from the *Swift* and SPM-1.5m telescopes, respectively. For both panels each light curve is represented with a different color, while the different symbols correspond to different instruments, as detailed in the legends. The legends also list offsets applied to each light curve. Photometry is shown in the AB mag system, with the exception of the *BV* bands, which are shown in the Vega system. The photometry shown has not been corrected for line-of-sight extinction.

Dessart, L., Blondin, S., Hillier, D. J., & Khokhlov, A. 2014, MNRAS, 441, 532

Faber, S. M., Phillips, A. C., Kibrick, R. I., et al. 2003, in Proc. SPIE, Vol. 4841, Instrument Design and Performance for Optical/Infrared Ground-based Telescopes, ed. M. Iye & A. F. M. Moorwood, 1657–1669

Fitzpatrick, E. L. 1999, PASP, 111, 63

Foley, R. J., Challis, P. J., Filippenko, A. V., et al. 2012, ApJ, 744, 38

Fremling, C., Sollerman, J., Taddia, F., et al. 2016, A&A, 593, A68

Ganeshalingam, M., Li, W., & Filippenko, A. V. 2011, MNRAS, 416, 2607

Goobar, A., Johansson, J., Amanullah, R., et al. 2014, ApJL, 784, L12

Goobar, A., Kromer, M., Siverd, R., et al. 2015, ApJ, 799, 106

Guy, J., Astier, P., Baumont, S., et al. 2007, A&A, 466, 11

Hayden, B. T., Garnavich, P. M., Kasen, D., et al. 2010a, ApJ, 722, 1691

Hayden, B. T., Garnavich, P. M., Kessler, R., et al. 2010b, ApJ, 712, 350

Hook, I. M., Jørgensen, I., Allington-Smith, J. R., et al. 2004, PASP, 116, 425

Hosseinzadeh, G., Sand, D. J., Valenti, S., et al. 2017, ArXiv e-prints, arXiv:1706.08990

Im, M., Choi, C., Yoon, S.-C., et al. 2015, ApJS, 221, 22

Kasen, D. 2010, ApJ, 708, 1025

Maoz, D., Mannucci, F., & Nelemans, G. 2014, ARA&A, 52, 107

Marion, G. H., Sand, D. J., Hsiao, E. Y., et al. 2015, ApJ, 798, 39

Marion, G. H., Brown, P. J., Vinkó, J., et al. 2016, ApJ, 820, 92

Masci, F. J., Laher, R. R., Rebbapragada, U. D., et al. 2017, PASP, 129, 014002

Miller, A. A., Laher, R., Masci, F., et al. 2016, The Astronomer's Telegram, 8907
Morozova, V., Piro, A. L., Renzo, M., et al. 2015, ApJ, 814, 63
Nugent, P. E., Sullivan, M., Cenko, S. B., et al. 2011, Nature, 480, 344
Ofek, E. O., Laher, R., Surace, J., et al. 2012, PASP, 124, 854
Oke, J. B., Cohen, J. G., Carr, M., et al. 1995, PASP, 107, 375
Olling, R. P., Mushotzky, R., Shaya, E. J., et al. 2015, Nature, 521, 332
Parrent, J. T., Thomas, R. C., Fesen, R. A., et al. 2011, ApJ, 732, 30
Parrent, J. T., Howell, D. A., Friesen, B., et al. 2012, ApJL, 752, L26
Phillips, M. M. 1993, ApJL, 413, L105
Piro, A. L., Chang, P., & Weinberg, N. N. 2010, ApJ, 708, 598
Piro, A. L., & Morozova, V. S. 2016, ApJ, 826, 96
Piro, A. L., & Nakar, E. 2014, ApJ, 784, 85
Poznanski, D., Prochaska, J. X., & Bloom, J. S. 2012, MNRAS, 426, 1465
Rabinak, I., & Waxman, E. 2011, ApJ, 728, 63
Schlafly, E. F., & Finkbeiner, D. P. 2011, ApJ, 737, 103
Shappee, B. J., Piro, A. L., Stanek, K. Z., et al. 2016a, ArXiv e-prints, arXiv:1610.07601
Shappee, B. J., Piro, A. L., Holoien, T. W.-S., et al. 2016b, ApJ, 826, 144
Silverman, J. M., & Filippenko, A. V. 2012, MNRAS, 425, 1917
Silverman, J. M., Ganeshalingam, M., Cenko, S. B., et al. 2012, ApJL, 756, L7
Starr, B. M., Luppino, G. A., Cuillandre, J.-C., & Isani, S. 2000, in Proc. SPIE, Vol. 3965, Sensors and Camera Systems for Scientific, Industrial, and Digital Photography Applications, ed. M. M. Blouke, N. Sampat, G. M. Williams, & T. Yeh, 58–69
Theureau, G., Hanski, M. O., Coudreau, N., Hallet, N., & Martin, J.-M. 2007, A&A, 465, 71
Thomas, R. C., Aldering, G., Antilogus, P., et al. 2007, ApJL, 654, L53
—. 2011, ApJ, 743, 27
Tonry, J. L. 2011, PASP, 123, 58
—. 2013, Philosophical Transactions of the Royal Society of London Series A, 371, 20120269
Valenti, S., Howell, D. A., Stritzinger, M. D., et al. 2016, MNRAS, 459, 3939
Vernet, J., Dekker, H., D'Odorico, S., et al. 2011, A&A, 536, A105
Whelan, J., & Iben, Jr., I. 1973, ApJ, 186, 1007
Zacharias, N., Finch, C. T., Girard, T. M., et al. 2013, AJ, 145, 44
Zhang, K., Wang, X., Zhang, J., et al. 2016, ApJ, 820, 67
Zheng, W., Silverman, J. M., Filippenko, A. V., et al. 2013, ApJL, 778, L15
Zheng, W., Shivvers, I., Filippenko, A. V., et al. 2014, ApJL, 783, L24